Heliyon 10 (2024) e30935

Contents lists available at ScienceDirect

Heliyon

journal homepage: www.cell.com/heliyon

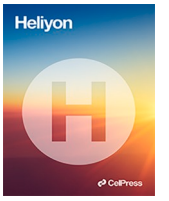

Research article

Insights on droplet drift and effective utilization of pesticide in "Third Pole" : Qinghai-Tibet Plateau of China

Hongyu Chen [1], Hua Weng [1], Haixia Zhu, Shuo Shen [**], Wei Li [*]

Academy of Agriculture and Forestry Sciences, Qinghai University, Key Laboratory of Qinghai -Tibetan Plateau Biotechnology (Qinghai University), Scientific Observing and Experimental Station of Crop Pest in Xining, Ministry of Agriculture, Key Laboratory of Agricultural Integrated Pest Management of Qinghai Province, Xining, 810016, Qinghai Province, PR China

ARTICLE INFO

Keywords:
Pesticide transport efficiency
Droplet drift
Crucial drift height
Droplet size distribution
Dispersion of droplet sizes

ABSTRACT

Crop protection pesticide spraying aims to greatly improve the utilization rate of pesticides. Controlling pesticides deposition requires a thorough understanding of the spatial behaviour of spray droplets.The Qinghai-Tibet Plateau, which is the headwaters of three largest water resources (Yangtze, Yellow and Lancang) in China, has exceptionally unique climatic characteristics. The goal is to reduce the amount of pesticides entering water resources. The wind tunnel experiment was used to validate the discrete phase method for tracking the trajectories. Cooperation between the smaller and larger droplets (greater than 150 μm) in the dense area around the nozzle can undoubtedly enhance the initial dispersion of droplet sizes. Droplet coalescence, which lowers the proportion of readily dispersed droplets, can greatly boost droplet deposition onto the target location.The crucial drift height is presented and clarified when droplets gradually disperse by identifying the descending length at which efficiency of mass transit starts towards decrease off quickly. The pesticide transport efficiency will not be enhanced by reducing the initial relative spread of droplets if the actual spray height surpasses the crucial drift height, and may even worsen drift loss. The temperature and relative humidity of the air have a greater influence on the evaporation losses of droplets smaller than 150 μm. In addition to providing information about pesticide spraying, the results of studies on droplet drift behaviors also suggest a method for controlling drift.

1. Introduction

Spray technology, which can break up liquids into numerous tiny droplets, is used in a variety of applications, including pesticide-controlled agricultural spraying, vehicle painting, spray cooling for thermal management, and fuel injectors for diesel engines [1]. Spraying chemical pesticides is a successful strategy for preventing biological invasion of agriculture and ensuring national food security [2]. Utilizing chemical insecticides sensibly can boost crop quality and agricultural production efficiency [3]. However, due to spatial drift caused by wind and interfacial runoff of crop leaves, the real deposition efficiency in the field is insufficient. The ISO [4] defines spray drift as "a part of the spray disperses into the atmosphere away from the region being treated, while another part drops to

* Corresponding author.
** Corresponding author.
E-mail addresses: wenzhanggz@163.com (S. Shen), qingyunguoqh@163.com (W. Li).
[1] These authors are co–first authors.

https://doi.org/10.1016/j.heliyon.2024.e30935
Received 8 November 2023; Received in revised form 1 May 2024; Accepted 8 May 2024
Available online 9 May 2024

the floor or vanishes rapidly." According to a recent announcement from China's Ministry of Agriculture, 40.6 percent of all pesticides used in that year will be applied to the three major food crops: wheat, corn, and rice. Spray drift can transport 40–55 percent of pesticide application levels off-site, according to the research, and field spray tests of 20–50 percent sprayed dosages support this claim [5]. Additionally, the authors compiled the spray several orchards' droplet drift and deposition ratios demonstrate that between 30 and 50 percent of the spray is lost to evaporation during the spraying operation [6]. Without a question, spray drift poses an unavoidable hazard to aquatic life, delicate plants, the environment, and human health. The spray droplet's initial relative span (RS), RS $= (D_{v90} - D_{v10})/D_{v50}$, also known as the original consistency of the droplet emitted through the nozzle, is simultaneously decreased [7]. This can significantly lessen reduction of drift and enhance the droppedlet's consistency upon deposit [8]. Currently, most agricultural nozzles create droplets with varying and uneven starting relative spans. In prior investigations, the effects of transfer of pesticides were therefore rarely examined in depth [9,10]. Therefore, in order to inform the design and optimization of nozzles.

In the field studies, the effectiveness of movement and accumulation of pesticides on different canopies was examined [11,12]. Through this methods and quantitative examination of chemicals, the effectiveness of pesticides' conveyance and use can be assessed [13]. However, the effectiveness of transportation can easily be impacted by the local sample technique and the unpredictable weather in the field [14]. Agriculture has made extensive use of numerical simulation because of its high controllability and flexibility. It is also possible to track the spatial route of fog droplets to learn more about the specifics of droplet deposition efficiency [15,16]. A number of numerical models have been put forth recently for land application, orchard management, and aerial spraying. These models effectively forecast the effectiveness of droplet deposition on various canopy layers. Spray equipments and operating variables can also be improved to increase coverage and effectiveness [17–19].

The majority of the study has been focused on starting diameter dispersion and ultimate effectiveness of deposition plants, both experimentally and numerically [20–22]. However, droplet distortion, collision, and evaporation between the nozzle and the target are absent. Droplet spatial behavior serves as a transitional link that can both represent the potential process of pesticide deposition and serve as feedback for the management of particle size [23–25]. The highest peak in the world, located in China's Qinghai-Tibet Plateau, is where the Yellow, Yangtze, and Lancang rivers originate. With regard to the planting area, it has unquestionable benefits, and it is perennially windy, dry, and rainier. However, pesticide application technology need more scientific direction [26,27].

This study concentrate on the droplet's spatial motion mechanism. When droplets leave the dense distribution close to the nozzle and progressively spread into the surrounding area, the trajectories of those droplets with various initial diameter distributions are monitored using proven discrete phase models. The droplet contact patterns in the dense zone are examined, along with how they affect the diameter distribution and efficacy of pesticide transport. At congested areas, contact mode of a droplet and its impact on particle size distribution and the effectiveness of pesticide delivery were evaluated. To limit the pesticide drift loss as droplets progressively diffused, critical drift height of droplets in varying particle dimensions was developed. Additionally, various atmospheric variables' effects on the evaporation behavior of droplets of various sizes were examined. This research will aid in understanding how pesticide droplets behave spatially and direct the development of regulatory mechanisms to lessen droplet formation.

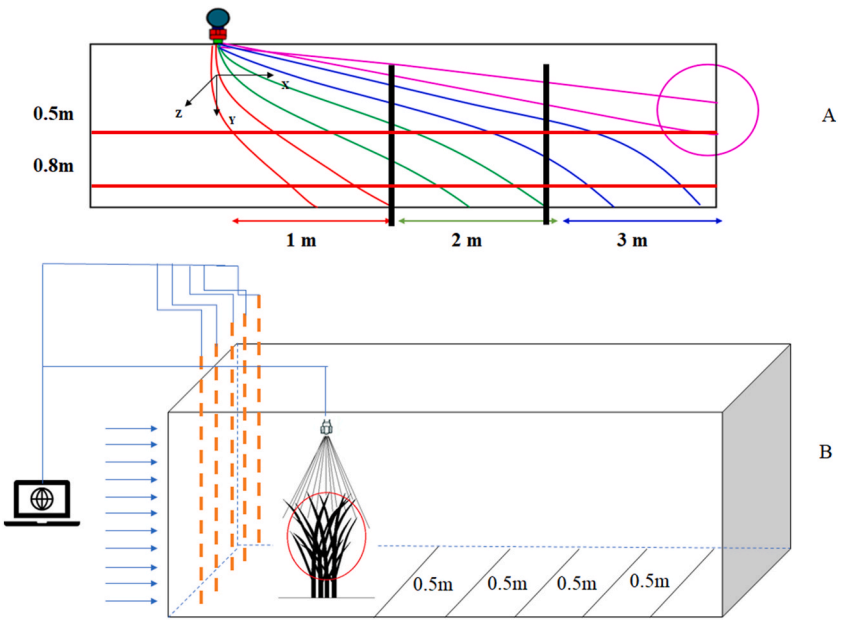

Fig. 1. Model of (A) The spatial trajectories of droplets traveling for 1.15 s (RS = 0.84, ua = 2.0 m/s, model results) and (B) Schematic of CFD numerical simulation.

2. Templates and methods

2.1. Templates of CFD

Between nozzle with the target surface, the droplet's spatial behavior and transport effectiveness were investigated. Chemical pesticides are sprayed in an open area during the application process. The computer domain is built as a rectangle in shape measuring 7.0 m by 1.5 m by 2.0 m. According to Fig. 1 A, splatter particles were introduced to area in place (0,0,1.0) in the form of a hollow cone with an initial velocity of 15 m/s and a liquid flow rate of 0.015 kg/s. In this investigation, aqueous solution with a densities of 976.91 kg/m^3, slickness of 2.02 mPa/s, and a surface stress of 0.018 N/m was employed to determine the characteristics. Crosswinds are considered to blow horizontally into the computation region with a homogeneous velocity distribution, and tiny velocity fluctuations within the height of the 1.5 m area are disregarded. Because atmospheric instability is not taken into account, the ground's temperature is shown to be uniform. Numerical simulation was conducted using the Eulerian-Lagrangian method because of the droplet's low volume fraction. The air velocity in the area is determined by resolving the conservation equations for mass, momentum, and energy [28]. The space motion trajectory of the droplet is tracked by solving the droplet motion equation. Spray droplet evaporation and random collision are also taken into account. Below is a diagram of the droplet phase's Lagrangian model [29]. The source term couples the air phase and the droplet phase together during the calculation.

The test materials are from Beijing Muyang Instrument Consumables Company, and the test site is located in Xiangride Town, Dulan County, Haixi Autonomous Prefecture, Qinghai Province.

2.1.1. Size distribution of the drops

The diameter dispersion at first of the droplet formed is described by Eq. (1) using Alousie function [30].

$$Y_{d_p} = e^{-\left(d_p/\overline{d}_p\right)^R} \tag{1}$$

Where Y_{dp} is the mass percentage of the droplet whose diameter is greater than d_p and d_p are the spray droplet's circumference that was injected. R is the diffusion parameter, while $\overline{d}_p$ is the average fog droplet diameter.

2.1.2. Motion model for droplets

The droplet inertia and various forces acting on the droplet are evaluated comprehensively to build a model for the movement trajectory of the spray droplet in the air, as indicated by Eqs. (2) and (3), [30].

$$\frac{du_p}{dt} = \frac{18\mu C_d Re}{24\rho_p d_p^2}\left(u_a - u_p\right) + \frac{g\left(\rho_p - \rho_a\right)}{\rho_p} + F_{other} \tag{2}$$

$$Re = \frac{\rho d_p \left|u_p - u_a\right|}{\mu} \tag{3}$$

Where g = 9.80 m s^{-2} (the gravitational quickening), ρ_a = 1.225 kg m^{-3} (density), μ = 1.7894 × 10^{-5} kg m^{-1}•s^{-1} (viscosity), Re represents relative Reynolds number, and F_{other} are the Safferman two forces acting on the droplet are lift and virtual mass.

Dynamic model was used to calculate the droplet drag coefficient. The idea that drag varies linearly with droplet deformation underlies the deformation of droplet in space motion (Eqs. (4) and (5)) [31].

$$C_d = C_{d,sphere}\left(1 + 2.632 y_d\right) \tag{4}$$

$$C_{d,sphere} = \begin{cases} 0.424, Re > 1000 \\ \dfrac{24}{Re}\left(1 + \dfrac{1}{6}Re^{2/3}\right), Re \le 1000 \end{cases} \tag{5}$$

Where, $C_{d,sphere}$ is the resistance coefficient of spherical fog drops, y_d is the deformation degree of fog drops, located between 0 (no deformation, spherical) and 1 (maximum deformation, disk shape).

2.1.3. Droplet random collision model

The O'Riourke's collision technique [32], which is predicated on the possibility that two droplet packets could collide in the same cell, is utilized in this study to include droplet collisions. Eq. (6) calculates the anticipated the quantity of times two droplet packets collide. Eq. (7)'s Poisson probability distribution determines the precise collision number n. Coalescence and bounce were the results of droplet-droplet collisions, The important collision parameter, Y, was where b was the actual collision value ascertained by a random integer, $b_{crit,}$ was established by Eqs. (8) and (9), [32]. Formula (9-10) [32], yields the critical collision parameter b_{crit}. The size and speed of the freshly formed droplet were determined by resolving the conservation equations for mass and momentum.

$$\overline{n} = \frac{n_2 \pi (d_L + d_S)^2 \left|u_L - u_S\right| \Delta t}{4V_c} \tag{6}$$

$$P(n) = e^{-n}\left(\frac{\overline{n}^{n}}{n!}\right) \tag{7}$$

$$b = \frac{(d_L + d_S)\sqrt{Y}}{2} \tag{8}$$

$$b_{crit} = \frac{d_L + d_S}{2}\sqrt{min\left(1.0, \frac{2.4}{We}\left\{\left(\frac{d_L}{d_S}\right)^{3} - 2.4\left(\frac{d_L}{d_S}\right)^{2} + 2.7\left(\frac{d_L}{d_S}\right)\right\}\right)} \tag{9}$$

$$We = \frac{\rho_p (u_L - u_S)^2 (d_L + d_S)}{2\sigma} \tag{10}$$

Among them, $\overline{n}$ is the average collision frequency between two micelle, the larger and smaller droplets are denoted by the subscripts L and S. △t stands for time, Vc stands for the mesh, and n2 is how many fog droplets there are in the smallest microclusters.

2.1.4. Model of droplet evaporation

Droplets evaporatively transfer mass and energy to the air by convection and latent heat, which are calculated by Eqs. (11) and (12) respectively. The mass transfer coefficient and heat transfer coefficient are calculated by Eqs. (13) and (14) respectively.

$$\frac{dm_p}{dt} = -A_p M_p k_c (C_s - C_\infty) \tag{11}$$

$$Sh = \frac{k_c d_p}{D_m} = 2.0 + 0.6 Re^{1/2} Sc^{1/3} \tag{12}$$

$$m_p C_p \frac{dT_p}{dt} = hA_p (T_a - T_p) - \frac{dm_p}{dt} h_{fg} \tag{13}$$

$$Nu = \frac{hd_p}{K} = 2.0 + 0.6 Re^{1/2} Pr^{1/3} \tag{14}$$

$m_p = 18.015$ kg kmol^{-1} (molecular weight), $cp = 4.182 \times 103$ J kg^{-1}•K^{-1}(thermal capacity of droplets), *kc* stands for mass transfer coefficient that is established by combining of equation, *h* is the coefficient of convective heat transmission (N_u), which stands for product of Re or *Pr*, where Pr is 0.0242 W m^{-1}•K^{-1}.

2.2. Trials with droplet spraying

Through a wind tunnel test, the CFD model's dependability was assessed. The average spray droplet diameter at various downwind points was observed, as seen in Fig. 1 B. The specific actions are:

Firstly, a laser particle size analyzer (Winner 318C, China) operating at 0.3 MPa pressure was used to assess the droplet diameter distribution at 0.1 m below the TR80 005 nozzle. As the basis for a numerical simulation. WSPs are positioned in various locations downwind of 1.5 m. 3.5 m at intervals of 0.5 m to capture drifting spray droplets. The nozzles were installed at a height of 0.7 m inside the wind tunnel. A method for generating wind energy comprises of several tiny axial fans. Behind the fan, a honeycomb net and a damper screen are added to maintain horizontal stability and consistent wind speed. The turbulence level is less than 5 %, and the velocity variation at the measuring location is less than 1 %. The thermal anemometer measures the wind speed, which is modified by changing the fan's input power. In spraying experiment, wind tunnel's wind speed is at 2.5 m/s, and after air flow had settled, spraying began for 3 s. WSPs are not gathered and tagged after spraying has ended until the drops of spray within the wind tunnel have fully settled. At last, the WSPs underwent scanning at a resolution of 600 dpi and 8 grayscale to provide photographs of the deposited droplets. The USDA-ARS developed DepositScan software [33] can automatically determine the deposit area of a droplet and determine the precise size of a single droplet. The applicability and accuracy of the CFD model were evaluated by measuring the average diameter of spray droplets deposited on three WSPs at each downwind position.

Table 1
Comparison of the mean diameter of deposited spray droplets in the experiments and CFD simulation.

Mean diameters (μm)	Downwind distance from the nozzle X (m)				
	1.5	2.0	2.5	3.0	3.5
Model results	180	160	140	122	115
Experiment results	183	164	150	138	119

3. Results and discussions

3.1. Model verification

When wind speed is 2.5 m/s, Table 1 depicts average diameter of spray droplets deposited on the wall. The average droplet diameter drops monotonically as the downwind distance from the nozzle increases, showing that the greater the drift distance, the smaller the droplet must be. The experimental droplet diameter in the wind tunnel was somewhat greater than that results of the simulation. The overlap of fog droplets on the WSPs may be the cause of the overestimation of the mean diameter obtained by image processing techniques. According to the ASAE S572 droplet size classification standard [34], the D_{v50} of the droplet produced by the TR80 005 nozzle at 0.3 MPa is 86.87 μm, which is classified as "Very Fine." The extended downwind location of the droplet provides a large overlapping coverage. At different downwind positions, the average diameter deviations between the simulation and experiment are usually less than 10 %, indicating some promise for predicting the spatial behavior of droplets from the nozzle using the CFD model.

3.2. The impact of falling distance on droplet behavior and transport effectiveness

The usual droplet dynamics characteristics and efficiency of transportation were explained using data of $D_{v50} = 144.12$ μm, RS = 0.83, and $u_a = 1.9$ m/s as an illustration. After leaving the nozzle, Fig. 2 depicts how pesticide droplets are transported. Fog droplets progressively spread out into the atmosphere thanks to the action of air from their initial dense dispersion. In Fig. 2, respectively, the variations of droplet total transport efficiency m_{ACUM}(%) and droplet mass fraction △m(%) with falling distances are portrayed. The cumulative mass fraction scarcely drops (approximately 0.35 %) when the drops fall 0.1 m away (Figur. 2), demonstrating that the droplets barely drift beyond 2 m in the downwind direction. However, there was a considerable change in the droplets' mass percentage of various sizes in this area, with a proportion of bigger droplets increasing and a percentage of smaller particles decreasing. Fig. 2 shows that in the thick area, fog droplet contact occurs frequently and primarily.

The cumulative mass fraction steadily drops as a result of droplet evaporation and little drift when the droplet falls continuously within the range y = 0.1, y = 0.5 m. (Fig. 2). Additionally, the difference in the mass fraction of droplets of various sizes is less than 5 %. This suggests that droplet dispersion weakens droplet contact. As demonstrated in Fig. 2, the majority of droplets can be placed in the desired area. As shown in Fig. 2, the cumulative mass fraction started to rapidly and drastically decrease as the fog droplets approached the height of y = 0.5 m, suggesting that they were steadily drifting outside the target area. For instance, the pesticide delivery effectiveness rapidly decreases from 97.10 to 52.88 % when the droplet drops from y = 0.5 m to y = 1.0 m and the initial RS is 0.84. This suggests that, as illustrated in Fig. 2, there is a crucial drift elevation (y*) for the move effectiveness of drops of insecticide during the application process. The majority of droplets can be deposited in the target location when the spray elevation is smaller than y*. If not, the droplets will gradually stray from the intended area, wasting and losing insecticides quickly.

The interaction behavior of droplets in dense regions and its impact on transport effectiveness will be further examined in the sections that follow. In order to give recommendations for field spraying, the critical drift height of various droplet sizes under various wind speeds and researchers looked into how droplets behaved when they evaporated in two common meteorological conditions.

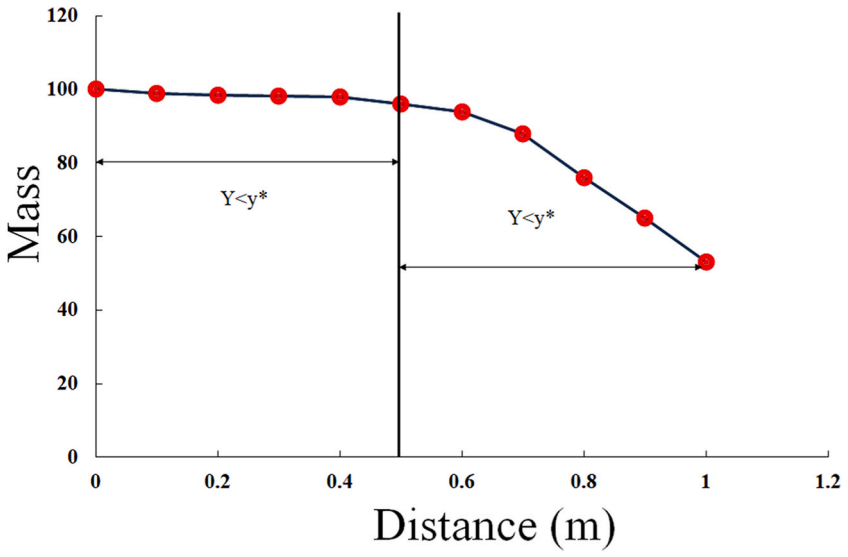

Fig. 2. Droplet behavior transition: Accumulative mass fraction of spray droplets with the falling distance (RS = 0.84 and u a = 2.0 m/s, model results).

3.3. Effects of droplet condensation on diameter distribution and mass transfer effectiveness

The behavior of different RS droplet contacts in the dense region between y = 0 and y = 0.1 m is examined in this section. In Table 4, the droplet's initial size distribution is displayed. Table 2 displays the characteristic droplet size D_{v10}, D_{v50}, and D_{v90} characteristics. As can be seen, the percentage of droplet dispersal between 100 and 200 μm increases as RS decreases. In the meantime, the proportion of droplets that were both larger than 200 μm and less than 100 μm steadily decreased. It suggests a more uniform dispersion of spray droplet diameters with smaller RS.

The change in fog drop mass fraction with various RS in the dense area is depicted in Table 4. The findings revealed that while the fraction of bigger droplets increased dramatically. There was a considerable reduction in the proportion of fog drops smaller than 150 μm. The evolution of droplet size and number in the initial release stream is depicted in S-Video in order to more thoroughly research the behavior of droplet interaction in this area. The findings reveal that while the number of droplets in the packet is greatly decreased, the droplet diameter less than 150 μm remains essentially unaltered. The number of droplets remained constant, but the diameter of those greater than 150 μm rose. No spray droplets strayed or totally melted after falling 0.1 m, it implies that the larger droplets combined with the smaller ones. Therefore, Individual mass fraction of droplets with different sizes is more likely to evolve as a result of droplets merging below 150 μm and above 150 μm. As seen in S-Video, the combined droplets formed when droplets of various sizes collide have a diameter that is more similar to that of large droplets. Additionally, it has been demonstrated that droplet agglomeration behavior can be promoted by increasing the size ratio of droplets [35,36].

Furthermore, the effects of RS about droplet fusion are investigated. While the mass decrease tendency is the reverse for droplets with diameters between 100 and 150 μm. It steadily rises as RS grows for droplets with sizes ranging from 50 to 100 μm. (Table 4). The reason behind this is that when RS values are high, there are more droplets distributed between 50 and 100 μm (like 1.30 and 1.08), making them easier to combine with other droplets during the collision process. The fraction of droplets with sizes between 100 and 150 μm, on the other hand, rises as RS lowers, leading to increased collisions between these droplets. It has been demonstrated that, particularly in the case of multi-nozzle spraying, by changing the original RS, the topic of droplet contact can be selectively changed.

It is remarkable how droplet merging affects the diameter distribution and mass transfer effectiveness. Droplet diameter distributions at various RS after convergence are shown in Table 4. The findings demonstrate that by lowering the number of small droplets, droplet aggregation in dense regions can increase droplet homogeneity. As seen in Table 4, differently, the percentage of droplets smaller than 100 μm decreases by 20.92 %, 15.37 %, 11.14 %, and 5.61 %., depending on the inception RS value. The improvement impact is evident for the droplet with a bigger ratio coefficient, but not for the droplet with a smaller ratio coefficient. Although droplet clustering behavior is more frequent when the relative ratio is bigger, even as the relative ratio falls, the droplet uniformity in the y = 0.1 m plane continues to rise, demonstrating that the improvement effect is constrained by the starting relative ratio difference.

Reducing smaller droplets can enhance drift resistance and decrease spatial drift loss in addition to enhancing the initial droplet distribution. Most droplets can be deposited in the target region in the range between y = 0.1 m and y = 0.5 m, mostly as a consequence of droplet mergers near the nozzle. Table 4 displays the droplet diameter distribution that was deposited on y = 0.5 m. The findings demonstrate that enhancing the uniformity of deposition can be achieved by lowering the initial spray droplet RS and the fraction of tiny droplets.

3.4. Different-sized droplet critical drift height

The crucial drift height is the drop distance at which the droplet mass fraction starts to quickly decline as the droplet approaches the target. This is mostly determined by the field spraying process's connection of droplet size and air speed. The migration of droplet off-target will not only reduce the effectiveness of the pesticide's use but also negatively impact the nearby delicate crops. Therefore, in order to establish a foundation for the create of the field spray high, the relationship between the critical drift height and droplet diameter, air velocity, and beginning droplet RS must be examined.

Fig. S1(a)~(c) displays how RS affects the distance and mass fraction of different droplets at which they fall. The findings demonstrate that, regardless of the size of the drag factor, proportion of fog drops with diameter between 100 and 150 μm exhibits a mildly declining trend in the range of y = 1/10 to 1/2 m. The portion of fog drops, however, starts to drastically decline when the airflow hits 2.0 m/s when the fog drops pass through the plane 0.5 m distant from the nozzle. According to the findings, after falling 0.5 m, droplets with a diameter of 100–150 μm start to stray outside the designated spot. Additionally, the droplet's spatial trajectory exhibits its drifting nature (as shown in "①" in Fig. 1A). As a result, for a velocity of the wind of 2.0 m/s, critical drift height of a 100–150 μm droplet is 1/2 m. In a similar vein, for different RS, the ration of fog drops reduces abruptly when 150–200 μm fog drops pass over y = 3/10 m plane, showing crucial drift high was 7/10 m. In Fig. 1A, drift behavior is displayed (labeled "②").

At comparison, the droplet that was deposited in the target zone between 200 and 250 μm has reduced drift loss. In general, RS

Table 2
The initial droplet size distribution of spray droplets with different RS.

D_{v10} (μm)	D_{v50} (μm)	D_{v90} (μm)	RS
62.17	129.99	232.77	1.30
71.11	140.18	222.43	1.08
80.76	142.89	200.95	0.84
99.01	149.38	188.37	0.60

largely affects the initial droplet's mass distribution and has little bearing on a single droplet's critical drift height. On the other hand, as droplet diameter decreases, the critical drift height drops quite dramatically.

However, as illustrated in Fig. S1(d)., RS has an impact on the cumulative transport efficiency of pesticides and is strongly correlated with the height of falling distance. The findings indicate that decreasing the benefits of RS has a favorable impact for transport efficiency in the vicinity of 0.8 m below the nozzle. However, as the droplet moves forward, the fall in RS will gradually have a detrimental effect on the effectiveness of the transport system. The drift loss of the drop at a distance of 1.0 m is 45.70 %, 46.81 %, 46.21 %, and 51.12 %, respectively, with the starting RS = 1.31, 1.17, 0.73, and 0.59. The findings demonstrate decreasing droplet's original RS value was advantageous for delivering pesticide within the constrained landing distance. The drift loss and ecological risk of pesticides will increase after real high of spray surpasses critical drift high of needed droplet.

Finding the sudden decrease points in transport efficiency, as Fig. S2(a)–(c) illustrates, helps to clarify how air velocity affects different droplet critical heights. According to the findings, droplets rarely move between 100 and 250 μm at 1 m/s of air speed. The mass spot decreases as the falling long increases with air velocity, increasing space drift loss as a result. In contrast, the critical height of small droplets is more significantly affected by wind speed, particularly for droplets that are smaller than 150 μm. Table 3 includes a summary of critical drift high of various drsoplets in a typical atmospheric spraying. The findings demonstrate that as air velocity and droplet diameter increase. Fig. S3(d) demonstrates how air velocity significantly affected the overall transport effectiveness of insecticides. The overall drift loss is 2.54, 2.94, 10.76, and 24.29 %, respectively, when the drop distance is 0.5 m. Air speed plays a major role in drift loss as the droplet continues to descend. The total drift loss increased to 8.37, 47.12, 85.50, and 96.01 %, respectively, when the droplet distance was raised to 1.0 m, demonstrating that the worse the field wind speed, the worse the drift loss. Spraying insecticides in the field is not recommended when the air flow rate is greater than 3 m/s, particularly for fog droplets that are smaller than 150 μm.

3.5. *Different-sized spray droplet evaporation loss*

The continual mass and heat exchange between fog droplets and the environment caused by space travel results in a decrease of fog droplet width or a lost of pesticide. Diffusion, which is primarily governed by droplet diameter, air temperature T, and relative humidity RH, regulates spatial evaporation of pesticide droplets.

Two typical atmospheric conditions are shown in Fig. S3(a) (moderate T and moderate RH; High T, low RH). Fig. S3(b) (c) displays the in line with the ratio of mass loss diameter reduction. The findings demonstrate that droplets with particle sizes greater than 150 μm have smaller diameter decrease rates and mass loss rates than other droplets. The evaporation loss of these droplets is therefore negligible and can be disregarded. However, in conditions of medium atmosphere, droplets smaller than 80 μm evaporate more quickly or perhaps completely. These droplets evaporate faster at higher ambient temperatures and lower relative humidity. This recommends that due to the significant evaporation loss, the first section of the droplet should be decreased as much as feasible. As opposed to this, droplets with diameters of 100 and 150 μm evaporate at rates that are more susceptible to atmospheric circumstances. When the temperature is 30 °C and the relative humidity is 60 %, the diameter reduction rate of these droplets is 4–14 %, while corresponding mass loss is 12–35 %. Diameter reduction rate and mass loss rate are 12–38 % and 31 and 76 %, respectively, at the extreme temperatures of 40 °C and 30 % relative humidity. In general, excellent wettability and translocation ability are exhibited by droplets between 100 and 150 μm on the target surface and within the leaf, respectively. Peoples can refrain from insecticides between fields when the weather is too arid. Contrarily, it is advised to combine useful adjuncts, with agricultural liquid first in order to modify the interfacial film's structure and prevent evaporation loss.

In addition to offering input on front-end design choices such as adjuvant synthesis and nozzle selection, the spatial behavior of the droplet also sets the stage for back-end application decisions like interface extension and internal translocation of plant leaves. In general, there are two ways to achieve the adjustment of space drift loss. One the one hand, the novel nozzles and adjuvants' creative designs can make fewer droplets susceptible to drift evaporation, lowering RS and enhancing the consistency of the first few drops. Making more droplets spread within the target's ideal diameter range is crucial for increasing the effectiveness of pesticide use. Conversely, collision behavior of droplets traveling through space can be controlled by active human involvement, encourage the binding of droplets that are prone to drifting, and minimize the loss of pesticides due to drift.

4. Conclusion

Under the nozzle, droplets have a distinctive spatial behavior as they transition from a dense to a scattered distribution, which significantly impacts the pesticides' ability to travel and their biological effects. The ratio of easily floating droplets is decreased, and the initial diameter distribution is more uniform, especially for droplets with large initial RS, in the vicinity of the nozzle at the droplet

Table 3
The critical drift heights of droplets with different diameters under various velocities.

Critical drift height (y*)	Ua = 1.0 m/s	Ua = 1.0 m/s	Ua = 1.0 m/s	Ua = 1.0 m/s
Dp = 100–150 μm	None	0.5 m	0.4 m	0.3 m
Dp = 150–200 μm	None	0.7 m	0.6 m	0.5 m
Dp = 200–250 μm	None	>1.0 m	0.8 m	0.7 m

Note: "None" means that droplets can almost deposit within 2 m downwind from the nozzle.

Table 4
Droplet coalescence and its impact on the diameter distribution and mass transport efficiency.

Falling distance (m)	Diameter (μm)	Mass fraction (%)			
		RS = 1.30	RS = 1.08	RS = 0.84	RS = 0.60
initial diameter distribution of injected droplets (0 m)	25	0	0	0	0
	75	34	25	18	10
	125	24	29	35	41
	175	18	25	32	44
	225	15	15	11	4
	275	4	3	2	0
	325	0	0	0	0
droplet diameter distribution after droplet interactions (0.1 m)	25	0	0	0	0
	75	12	9	8	5
	125	21	22	23	25
	175	25	28	34	42
	225	20	23	23	22
	275	15	13	7	4
	325	0	0	0	0
droplet diameter distribution when droplets are falling a distance of 0.5 m	25	0	0	0	0
	75	9	8	6	4
	125	19	18	20	22
	175	23	27	32	39
	225	21	21	24	23
	275	15	12	10	6
	325	4	3	2	1

interaction area where droplets smaller than 150 μm are more likely to merge with droplets larger than 150 μm. The droplet drift resistance can be increased by reducing the droplet size to less than 100 μm. At various wind speeds, critical drift height of droplets with sizes between 100 and 250 μm was found. The amount of droplets smaller than 150 μm that evaporate is greatly influenced by atmospheric conditions. By controlling the factors of droplet fusion, deposition uniformity, droplet drift and evaporation in this study, We can significantly increase the rate at which pesticides are used, decrease the amount of pesticides used, and safeguard the Qinghai Plateau's ecological environment.

Funding

This study was funded by Applied Basic Research Project of Qinghai Province (Grant No. 2023-ZJ-930 M).

Ethical approval

This article does not contain any studies with human participants or animals performed by any of the authors.

Data availability

No data was used for the research described in the article.

CRediT authorship contribution statement

Hongyu Chen: Writing – original draft, Software, Methodology, Data curation, Conceptualization. **Hua Weng:** Software, Methodology, Data curation, Conceptualization. **Haixia Zhu:** Supervision, Resources. **Shuo Shen:** Writing – original draft, Visualization, Supervision. **Wei Li:** Writing – review & editing.

Declaration of competing interest

The authors declare that they have no known competing financial interests or personal relationships that could have appeared to influence the work reported in this paper.

Appendix A. Supplementary data

Supplementary data to this article can be found online at https://doi.org/10.1016/j.heliyon.2024.e30935.

References

[1] D. Hua, X. Zheng, K. Zhang, Z. Zhang, Y. Wan, X. Zhou, Y. Zhang, Q. Wu, Assessing pesticide residue and spray deposition in greenhouse eggplant canopies to improve residue analysis, J. Agric. Food Chem. 68 (43) (2020) 11920–11927.
[2] X. Zhao, H. Cui, Y. Wang, C. Sun, B. Cui, Z. Zeng, Development strategies and prospects of nano-based smart pesticide formulation, J. Agric. Food Chem. 66 (26) (2018) 6504–6512.
[3] H. Guo, Y. Xia, J. Jin, C. Pan, The impact of climate change on the efficiency of agricultural production in the world's main agricultural regions, Environ Impact Asses 97 (2022) 106891.
[4] ISO 22856, Equipment for Crop Protection-Laboratory Measurement of Spray Drift-Part 1: Wind Tunnel, 2008.
[5] O. Kira, Y. Dubowski, R. Linker, In-situ open path FTIR measurements of the vertical profile of spray drift from air-assisted sprayers, Biosyst. Eng. 169 (2018) 32–41.
[6] G. Garcia-Santos, G. Feola, D. Nuyttens, J. Diaz, Drift from the use of hand-held knapsack pesticide sprayers in boyacá (Colombian Andes), J. Agric. Food Chem. 64 (20) (2016) 3990–3998.
[7] M. Massinon, N.D. Cock, S.O.T. Salah, F. Lebeau, Reduced span spray-Part 1:retention, Asp. Appl. Biol. 132 (2016) 1–8.
[8] U.T. Schönenberger, J. Simon, C. Stamm, Are spray drift losses to agricultural roads more important for surface water contamination than direct drift to surface waters? Sci. Total Environ. 809 (2022) 151102.
[9] Y. Seung-Hwa, Y. Young-Tae, C. Yong, R.A. Dafsari, J. Lee, Effect of injection angle on drift potential reduction in pesticide injection nozzle spray applied in domestic agricultural drones, J. Biosyst Eng. 46 (2021) 129–138.
[10] A. Connolly, K. Jones, K.S. Galea, I. Basinas, L. Kenny, P. McGowan, M. Coggins, Exposure assessment using human biomonitoring for glyphosate and fluroxypyr users in amenity horticulture, Int. J. Hyg. Envir Heal. 220 (6) (2017) 1064–1073.
[11] H. Se-Woon, L. Zhao, H. Zhu, CFD simulation of pesticide spray from air-assisted sprayers in an apple orchard: tree deposition and off-target losses, Atmos. Environ. 175 (2018) 109–119.
[12] R. Li, M. Trevor Scholtz, F. Yang, J.J. Sloan, A multimedia fate and chemical transport modeling system for pesticides: I. Model development and implementation, Environ. Res. Lett. 6 (2011) 034029.
[13] E. Cerruto, G. Manetto, D. Longo, S. Failla, R. Papa, A model to estimate the spray deposit by simulated water sensitive papers, Crop Prot 124 (2019) 104861–104871.
[14] O. Gaonkar, I.M. Nambi, G.S. Kumar, Biodegradation kinetics of dichlorvos and chlorpyrifos by enriched bacterial cultures from an agricultural soil, Bioremediat J 23 (4) (2019) 259–276.
[15] Y. Wang, M. Zhu, T. Shi, X. Ma, X. Wu, Q. Li, R. Hua, Construction of a novel fluorescent nanocarrier with double hollow shells for pH-controlled release of imidacloprid and its distribution and transport in bok choy, Ecotox Environ Safe 246 (2022) 114132.
[16] Y. Xiang, G. Zhang, Y. Chi, D. Cai, Z. Wu, Fabrication of a controllable nanopesticide system with magnetic collectability, Chem Eng J 328 (2017) 320–330.
[17] L. Huang, Z. Wang, K.A. Cupp-Sutton, K. Smith, S. Wu, Spray-capillary: an electrospray-assisted device for quantitative ultralow-volume sample handling, Anal. Chem. 92 (1) (2019) 640–646.
[18] M. Seesen, R.G. Lucchini, S. Siriruttanapruk, R. Sapbamrer, S. Hongsibsong, S. Woskie, P. Kongtip, Association between organophosphate pesticide exposure and insulin resistance in pesticide sprayers and nonfarmworkers, Int. J. Env Res. Pub He. 17 (21) (2020) 8140–8149.
[19] X. An, X. Liu, J. Jiang, L. Lv, F. Wang, S. Wu, X. Zhao, Exposure risks to pesticide applicators posed by the use of electric backpack sprayers and stretcher-mounted sprayers in orchards, Hum. Ecol. Risk Assess. 4 (2019) 2288–2301.
[20] S. Pascuzzi, V. Bulgakov, F. Santoro, A.S. Anifantis, S. Ivanovs, I. Holovach, A study on the drift of spray droplets dipped in airflows with different directions, Sustainability 12 (11) (2020) 4644–4652.
[21] R. Sijs, D. Bonn, The effect of adjuvants on spray droplet size from hydraulic nozzles, Pest Manag. Sci. 76 (10) (2020) 3487–3494.
[22] B.K. Munjanja, Y. Naudé, P.B.C. Forbes, A review of sampling approaches to off-target pesticide deposition, Trends Environ Anal 25 (2020) e00075.
[23] F. Huang, Z. Chen, Z. Li, Z. Gao, J.J. Derksen, A. Komrakova, Numerical study of drop behavior in a pore space, Chem. Eng. Sci. 233 (2021) 116351.
[24] L. Rousseau, C. Lempereur, M. Orain, O. Rouzaud, O. Simonin, Droplet spatial distribution in a spray under evaporating and reacting conditions, Exp Fluids 62 (2021) 379–388.
[25] K.S. Raghuram Gannena, D. Chaitanya Kumar Rao, D. Roy, A. Kumar, S. Basu, Bubble dynamics and atomization in evaporating polymeric droplets, J. Fluid Mech. 76 (894) (2022).
[26] D. Han, J. Huang, L. Ding, G. Zhang, X. Liu, C. Li, F. Yang, Breaking the ecosystem balance over the Tibetan plateau, Earth's Future 10 (10) (2022). No. EF002890.
[27] H. Li, W. Song, Spatiotemporal distribution and influencing factors of ecosystem vulnerability on Qinghai-Tibet Plateau, Int. J. Env Res. Pub He. 18 (12) (2021) 6508–6517.
[28] B. Bugbee, O. Monje, B. Tanner, Quantifying energy and mass transfer in crop canopies: sensors for measurement of temperature and air velocity, Adv. Space Res. 18 (4–5) (1996) 149–156.
[29] C. Kaliakatsos, S. Tsangaris, Motion of deformable drops in pipes and channels using Navier–Stokes equations, Int. J. Numer Meth Fl. 34 (7) (2000) 609–626.
[30] P. Gonzalez-Tello, F. Camacho, J.M. Vicaria, P.A. González, A modified Nukiyama–Tanasawa distribution function and a Rosin-Rammler model for the particle-size-distribution analysis, Powder Technol. 186 (3) (2008) 278–281.
[31] R.W. Breault, S.L. Rowan, E. Monazam, K.T. Stewart, Lateral particle size segregation in a riser under core annular flow conditions due to the Saffman lift force, Powder Technol. 299 (2016) 119–126.
[32] G. Lendvay, Mechanism change in the dynamics of the O′+ O2 → O′O + O atom exchange reaction at high collision energies, J. Phy Chem A. 123 (47) (2019) 10230–10239.
[33] H. Zhu, M. Salyani, R.D. Fox, A portable scanning system for evaluation of spray deposit distribution, Comput. Electron. Agric. 76 (1) (2011) 38–43.
[34] ISO, ASAE-S572 Spray Tip Classification by Droplet Size, 2009.
[35] A.G. Islamova, S.A. Kerimbekova, N.E. Shlegel, P.A. Strizhak, Droplet-droplet, droplet-particle, and droplet-substrate collision behavior, Powder Technol. 403 (2022) 117371.
[36] S. Li, F. Chu, J. Zhang, D. Brutin, D. Wen, Droplet jumping induced by coalescence of a moving droplet and a static one: effect of initial velocity, Chem. Eng. Sci. 211 (2020) 115252.